Realistic Micro-Doppler Simulation of Pedestrians in Automotive Radar Applications

Peter Mergenthaler[1], Oliver Sura[1], Eva Dorschky[2], Christian Schüßler[2], Marcel Hoffmann[2], Martin Vossiek[1]
[1]*Institute of Microwaves and Photonics (LHFT), Friedrich-Alexander-Universität Erlangen-Nürnberg (FAU), Germany*
[2]*fiveD GmbH, Erlangen, Germany*
{peter.mergenthaler, oliver.sura, martin.vossiek}@fau.de
{eva.dorschky, christian.schuessler, marcel.hoffmann}@five-d.ai

***Abstract*—Detecting vulnerable road users (VRUs), such as pedestrians, is crucial in automotive applications. Radar systems, with their ability to capture micro-Doppler signatures, are particularly well suited for this task. To evaluate their performance in complex scenarios and edge cases, realistic simulation tools are indispensable. In this paper, we introduce a method for realistically simulating radar raw data of moving pedestrians in arbitrary scenarios. For synthesizing the digital pedestrian, we captured the human gait with a state-of-the-art motion capture system. The extracted gait data was then used to animate a virtual human based on the SMPL-X model. Leveraging a digital radar twin, we generated matching synthetic radar raw data of the measurement scenario. Through the analysis and comparison of both measured and simulated data, the accuracy of the proposed simulation approach is validated. The simulation proved to be a powerful framework for designing and testing radar systems and VRU classification algorithms, ensuring reliable operation in complex real-world environments.**

***Index Terms*—Automotive radar, simulation, micro-Doppler, digital-twin, pedestrian.**

I. Introduction

The detection and classification of vulnerable road users (VRUs) is one of the most critical tasks in automotive perception. Radar sensors are particularly well suited for this task due to their ability to measure Doppler shifts – and consequently, the velocity of surrounding objects – while remaining robust against adverse environmental conditions such as poor weather and low lighting [1]. Many recent signal processing algorithms for VRU detection, such as [2] and [3], leverage neural networks. These approaches require diverse datasets, which are challenging to collect and must be regenerated for each different radar sensor. The authors of [3] demonstrated that their neural network, trained on automatically labeled data, outperformed one trained on manually labeled data due to the increased dataset size, despite imperfections in the automatic labeling process. Training and validating algorithms in edge-case scenarios pose significant challenges. Most real-world measurement datasets rarely contain such critical instances, as they would endanger the life of test subjects. This includes sudden street crossings or vehicles reversing into pedestrians. Such scenarios can only be replicated with dummies, which do not serve as realistic radar targets.

This work was partly funded by Deutsche Forschungsgemeinschaft (DFG, German Research Foundation)—SFB 1483–Project-ID 442419336, EmpkinS.

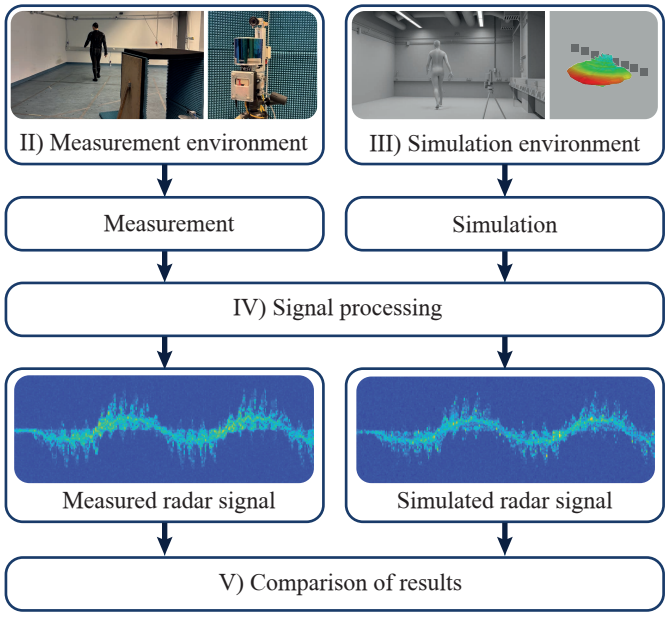

Fig. 1: The radar signature of a walking pedestrian is recorded while the motion is tracked using an optical motion capture system. A digital twin of the setup is then used to simulate radar raw data based on the motion capture data. Both simulated and real-world data are processed using the same signal processing chain to enable a fair comparison.

To address this challenge, we propose generating these datasets through a sophisticated simulation pipeline. This approach enables the creation of realistic, inherently labeled radar data. However, to establish the validity of the simulation, an in-depth analysis is required, with particular emphasis on the micro-Doppler components of pedestrian motion. To validate our simulation approach, we followed the procedure outlined in Fig. 1. We recorded a walking pedestrian using a typical automotive radar while simultaneously capturing the biomechanical model with a marker-based optical motion tracking system (Sec. II). This motion data was then used to animate a virtual human body hull placed into a 3D model of the measured laboratory. Further details on the simulation environment and the digital radar twin used to generate the radar raw data are provided in Sec. III. Subsequently, both signals

Fig. 2: Measurement environment: The pedestrian, wearing a motion capture suit with optical markers, follows a trajectory (green) radially toward the radar (red). Mounted next to the radar on the tripod is a camera for visual reference and a LiDAR, which remained turned off during the measurement.

are processed using the same pipeline presented in Sec.IV, ensuring a fair comparison. The quality of the simulation is then analyzed and compared to the measurement in Sec. V. Finally, Sec. VI presents conclusions and future perspectives on generating synthetic datasets for VRU detection.

II. Measurement Environment

To evaluate the simulation's capabilities, the quality of the recorded data is of paramount importance. A perfectly matched digital twin is essential for identifying residual artifacts in the simulation and determining whether it can be reliably used to generate artificial datasets. Thus, we conducted a high quality reference measurement campaign for recording the radar raw data, as depicted in Fig. 2. The pedestrian walked approximately 4 meters toward the radar (red) while being tracked by motion capture cameras (blue) before turning around. This trajectory was repeated twice, resulting in a measurement duration of approximately 12 s. Since this study focuses on analyzing direct human reflections, the radar was surrounded by absorbing material to mitigate interference from multipath effects in the measurements.

A. FMCW-MIMO Radar

Raw data acquisition was performed using the Texas Instruments IWR6843ISK radar, mounted on a tripod (cf. Fig. 1). The radar is configured as a frequency-modulated continuous wave (FMCW) chirp sequence radar with the parameters in Tab. I. Although the radar features three transmitting (TX) and four receiving (RX) antennas, only two TX antennas in a time division multiplex (TDM) scheme and one RX antenna were used, since solely micro-Doppler components were investigated. The radar raw data was streamed via a custom Robot Operating System (ROS) interface, with a timestamp assigned to each frame. Additionally, the radar's outer casing was tagged with optical markers to precisely determine its position within the optical motion capture coordinate system.

TABLE I: Radar Parameters

Parameter	Value
Carrier frequency	60 GHz
Bandwidth	716.86 MHz
Number of chirps per TX antenna	140
Measurement duration	27.5 ms
Velocity resolution	$0.091\,\mathrm{m\,s^{-1}}$
Maximum unambiguous velocity	$6.36\,\mathrm{m\,s^{-1}}$
Range resolution	0.21 m
Maximum unambiguous range	26.78 m
Frame rate	20 Hz

B. Optical Motion Tracking

Optical motion tracking systems are the gold standard for capturing complex motions, such as human gait. In this work, we used an optical motion tracking system from OptiTrack[1] to record the biomechanical movement of a walking pedestrian. The room is equipped with 12 infrared cameras (blue) evenly spaced throughout the laboratory to ensure full coverage of the pedestrian's trajectory (green) toward the radar and back. The pedestrian was wearing a motion capture suit fitted with 37 optical markers, distributed across the body to accurately capture limb movements. The tracking data was recorded at a frame rate of 120 Hz, ensuring precise tracking of even subtle micro-motions. While the optical motion tracking cameras capture data synchronously, the radar and visual camera were recorded separately and therefore required additional synchronization. To achieve this, the tracking data was also streamed to the same recording device as the radar data via a ROS interface, ensuring a unified timestamp for all recorded measurements.

III. Simulation Environment

To recreate the measurement scenario, we require a digitized human model and a virtual 3D representation of the measurement environment to accurately capture the real-world reflection behavior of electromagnetic wave propagation. The human model is generated based on the SMPL-X model [4], with parameters and mesh shape carefully selected to closely match the pedestrian's real physiology. The virtual human was then animated using kinematic data extracted from optical motion capture, processed in Blender. Since the walking pedestrian is already spatially and temporally aligned with the radar, the 3D virtual environment of the laboratory is transformed to share the same coordinate origin and orientation as the motion capture system. An example of a rendered frame depicting the walking pedestrian in the laboratory is shown in Fig. 3. Radar simulations were conducted using an advanced physical-optics (PO)-based ray-tracing approach developed by fiveD[2], which was adapted from [5]–[7]. Since the focus of this paper is only on the micro-Doppler components, the digital twin of the real-world radar is replicated utilizing one receiving and two transmitting antennas to match the time division multiplex scheme of the

[1]NaturalPoint, Corvallis, USA, https://optitrack.com/
[2]fiveD GmbH, Erlangen, Germany, https://fived.ai/

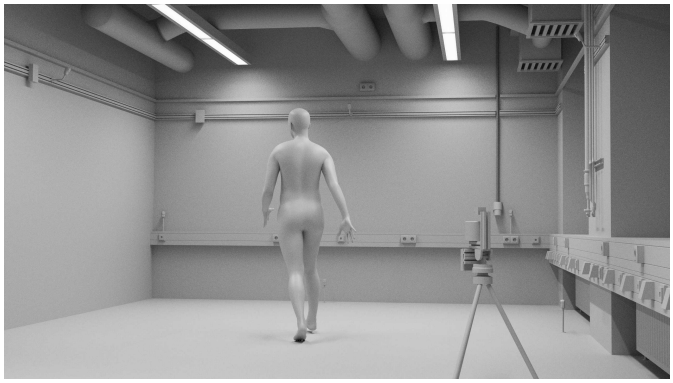

Fig. 3: Virtual environment: Digital twin of the pedestrian inside the laboratory, with the radar mounted on a tripod. The coordinate system of the motion capture data and the virtual environment are aligned, ensuring that the trajectory and radar position accurately replicate the real-world scenario.

real-world radar. Although the simulator features sophisticated electromagnetic material models, the objects within this study were modeled as perfectly electrically conductive. While this provides a reasonable approximation for the specular reflection behavior of human skin at millimeter-wave frequencies [8], it does not fully capture the actual materials present in the laboratory. However, given that static targets are filtered out during signal processing, this simplification only has a minor effect on the micro-Doppler components of the simulated pedestrian. A comprehensive matching of real-world material properties in the simulation lies beyond the scope of this work. Thus, future studies have to place a special emphasis on capturing and evaluating the reflectance behavior of the pedestrian, due to its critical role in realistic radar target modeling of vulnerable road users.

IV. Signal Processing

As a first step, the measured radar raw data is used to obtain a rough power estimate of the radar's noise floor. Since the simulation is conducted without noise, this estimate is then added to the simulated radar raw data as Gaussian noise before transforming both time-domain signals into range domain using a fast Fourier transform (FFT). Next, static targets are suppressed by subtracting the mean in the slow-time dimension, followed by a Doppler FFT. The overall signal processing chain is summarized in Fig. 4. Because the laboratory's back walls act as dihedral reflectors, both the measured and simulated range-Doppler frames are cropped in range to exclude resulting multipath and double-bounce effects. The processed range-Doppler frames are then stored for later evaluation. Additionally, each range-Doppler frame is reduced to a single slice by computing the maximum Doppler value over range. Accumulating these slices over time produces a Doppler-time spectrogram (DTS), which visualizes velocity components over time – a powerful tool for analyzing the pedestrian's movement sequence. To ensure a fair comparison, the absolute power of both measured and simulated data

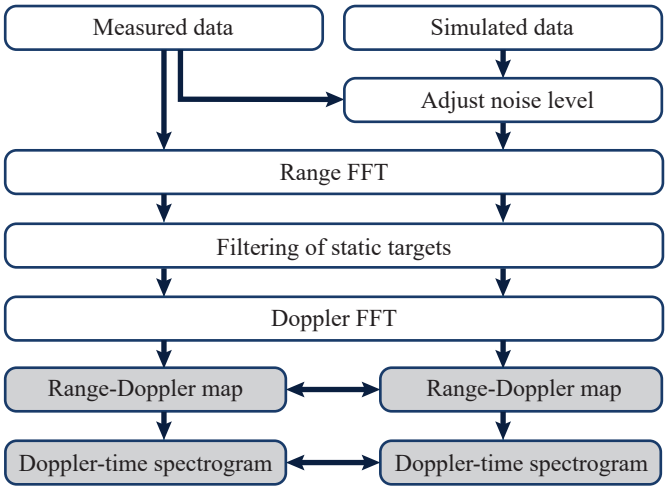

Fig. 4: Signal processing chain for measured and simulated radar data. Range-Doppler maps are computed via Fast Fourier Transform (FFT) and accumulated into a Doppler-time spectrogram (DTS), both serving as key aspects of the comparison.

is normalized to $0\,\mathrm{dB}$, as the transmit power of the simulation has not been matched to its real-world counterpart.

V. Comparison of Results

A. Range-Doppler Map

A subset of the measured and generated range-Doppler frames, along with the corresponding camera images, is depicted in Fig. 5. In the first row (Fig. 5a-c), the pedestrian is walking away from the radar, resulting in primarily positive velocity components. Additional components with a negative Doppler shift are visible in both the measurement and the simulation. These originate from the back swinging arm of the pedestrian, which is further analyzed in Sec. V-B. The peaks in the measured and simulated range-Doppler maps align almost perfectly, with only a slight mismatch in amplitude distribution. In the middle row (Fig. 5d-f), another measurement of the walking cycle is shown. Compared to Fig. 5a, in this case, both feet are stationary, thus resulting in a more compact Doppler spread, as the legs are the fastest-moving components in human gait. Also, one noticeable effect in the center and the upper frame is that the amplitudes of the simulated micro-Doppler components seem to be slightly smeared along the Doppler dimension, when compared to the measurement. This discrepancy may be attributed to the pure metallic material model used for the digital human, which does not fully capture real-world reflection behavior and will be investigated further in future work. Since changes in movement are particularly important when analyzing edge-case scenarios, the bottom row (Fig. 5g-i) depicts the turning point of the trajectory. All reflection points are centered around the zero Doppler-bin, as the pedestrian performs a 180-degree rotation, leading to a stationary torso. The symmetric shape results from the swinging limbs, where one limb moves toward the radar while the other moves away with nearly the same

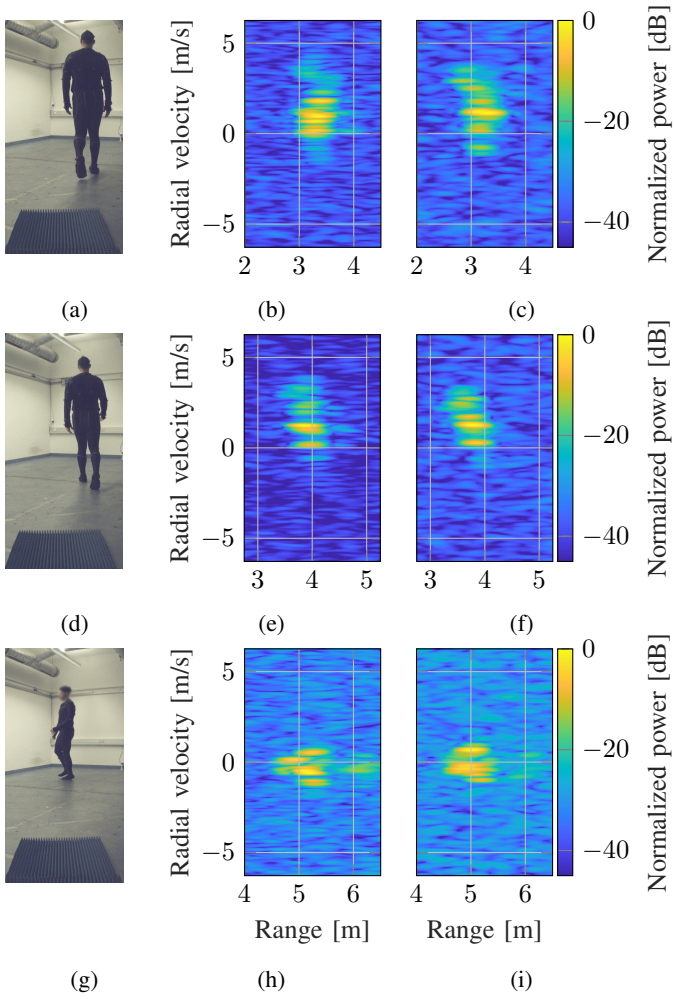

Fig. 5: Selected range-Doppler frames of a walking pedestrian. Reference camera images are shown in the left column (a, d, g), the corresponding measured range-Doppler maps in the center column (b, e, h), and the matching simulated range-Doppler maps in the right column (c, f, i).

velocity. Although minor differences in reflection points can be observed, the overall relative amplitudes and reflection positions match remarkably well.

B. Doppler-Time Spectrogram

The Doppler-time spectrogram of the measured and simulated data are compared in Fig. 6. For further analysis, the marker data from the motion capture system, corresponding to the torso, feet and hands, is shown in Fig. 6c. Since the measurement started in a static pose (as seen in Fig. 2), no velocity components are initially visible in any of the three plots. Once the pedestrian begins walking at approximately $16.2\,\mathrm{s}$, the Doppler components of different body parts start to spread due to their varying radial velocities relative to the radar. These components are clearly distinguishable. The walking distance in the laboratory was limited to approximately $4\,\mathrm{m}$, resulting in the recording of about five foot steps that are clearly visible due to their high radial velocity. After walking toward the radar, the pedestrian turned around and walked back to the starting point, effectively repeating the measurement. A single foot step can be clearly observed between from $18.0\,\mathrm{s}$ to $18.5\,\mathrm{s}$. During this phase, the torso moves with an almost constant velocity, serving as the strongest reflection point due to its higher radar cross-section. At the starting point, both feet (marked in red and green) are on the ground while the arms are extended. Immediately after, the hands begin moving in opposite directions: the right hand (green) exhibits a positive velocity relative to the torso, while the left hand (violet) exhibits a negative velocity. Whereas the left foot (orange) remains on the ground, the right foot begins its swing, producing a high negative velocity component, which is clearly visible in the DTS. Due to the periodic nature of human walking, this cycle repeats with left and right limbs interchanged. Although not immediately identifiable without motion capture reference data, the pedestrian's hands are visible in the spectrogram, sometimes even causing negated Doppler components, such as at $24.2\,\mathrm{s}$. One noticeable difference between the measured and simulated DTS is the smearing effect, also observed in Fig. 5f. For example, during the walk from $22\,\mathrm{s}$ to $26\,\mathrm{s}$, the measured DTS shows discrete scattering centers along the Doppler dimension, leading to velocity components with amplitudes near the noise floor. In contrast, the simulated DTS exhibits a broader spread of velocity components, distinguishable above the noise floor. Despite these minor differences, the relative amplitudes in the measured and simulated data match remarkably well. By leveraging the ray-tracing approach used in the simulation, the information stored in the rays can be further utilized to differentiate between components. This presents a powerful tool for advanced radar data analysis, paving the way for the development of next-generation signal processing algorithms.

VI. Conclusion

In this work, we recorded the radar signature of a walking pedestrian and simultaneously captured its movement using a high-precision optical motion tracking system. The extracted skeletal motion was used to animate a human body mesh model, enabling the creation of an almost identical replica of the real-world measurement scenario, along with a virtual representation of the radar. Using this digital twin, we simulated radar raw data with a ray-tracing-based radar simulation tool. Both the measured and simulated radar data were processed through the same processing chain, and the resulting range-Doppler maps and Doppler-time spectrograms were analyzed. Our findings demonstrate that the simulated data closely matches the real-world reference, confirming the feasibility of realistic radar simulations for pedestrian detection in automotive applications. For future work, we plan to further investigate the amplitude distribution of targets to enhance the similarity between measurement and simulation. Based on these findings, the virtual environment can be leveraged to simulate edge-case scenarios that are challenging or impossible to capture in real-world measurements due to

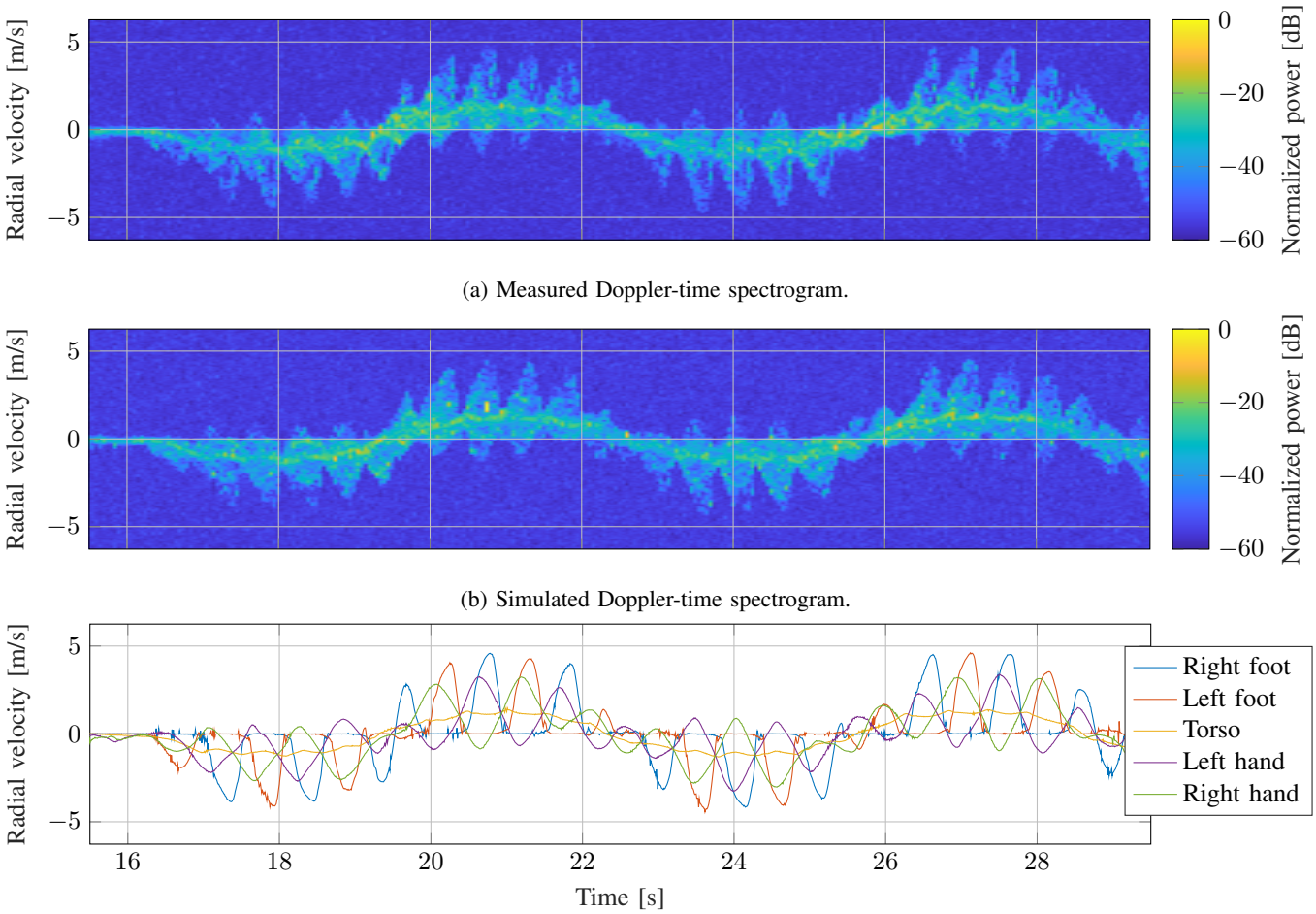

(a) Measured Doppler-time spectrogram.

(b) Simulated Doppler-time spectrogram.

(c) Measured motion capture reference data.

Fig. 6: Visual comparison between measured Doppler-time spectrogram (a) and simulated Doppler-time spectrogram (b). For reference, the velocities of the recorded optical marker data with respect to the radar are depicted in (c).

physical and ethical constraints. Furthermore, radar parameters and configurations can be optimized in the virtual environment to minimize costs and accelerate workflows. The simulated pedestrians can be generated from existing human motion capture datasets, such as [9] or entirely virtual motion models can be used to create synthetic radar datasets. Ultimately, these virtual datasets can be used to train and test algorithms, contributing to the advancement of VRU safety in autonomous systems.

References

[1] J. Hasch et al., "Millimeter-Wave Technology for Automotive Radar Sensors in the 77 GHz Frequency Band," in IEEE Transactions on Microwave Theory and Techniques, vol. 60, no. 3, pp. 845-860, March 2012, doi: 10.1109/TMTT.2011.2178427.

[2] R. Pérez, F. Schubert, R. Rasshofer and E. Biebl, "Single-Frame Vulnerable Road Users Classification with a 77 GHz FMCW Radar Sensor and a Convolutional Neural Network," 2018 19th International Radar Symposium (IRS), Bonn, Germany, 2018, pp. 1-10, doi: 10.23919/IRS.2018.844812 6.

[3] M. Dimitrievski, I. Shopovska, D. V. Hamme, P. Veelaert and W. Philips, "Weakly Supervised Deep Learning Method for Vulnerable Road User Detection in FMCW Radar," 2020 IEEE 23rd International Conference on Intelligent Transportation Systems (ITSC), Rhodes, Greece, 2020, pp. 1-8, doi: 10.1109/ITSC45102.2020.9294399.

[4] G. Pavlakos et al., "Expressive Body Capture: 3D Hands, Face, and Body From a Single Image," 2019 IEEE/CVF Conference on Computer Vision and Pattern Recognition (CVPR), Long Beach, CA, USA, 2019, pp. 10967-10977, doi: 10.1109/CVPR.2019.01123.

[5] C. Schüßler, M. Hoffmann, J. Bräunig, I. Ullmann, R. Ebelt and M. Vossiek, "A Realistic Radar Ray Tracing Simulator for Large MIMO-Arrays in Automotive Environments," in IEEE Journal of Microwaves, vol. 1, no. 4, pp. 962-974, Oct. 2021, doi: 10.1109/RadarConf2351548.2023.10149641.

[6] C. Schüßler et al., "Achieving Efficient and Realistic Full-Radar Simulations and Automatic Data Annotation by Exploiting Ray Meta Data from a Radar Ray Tracing Simulator," 2023 IEEE Radar Conference (RadarConf23), San Antonio, TX, USA, 2023, pp. 1-6, doi: 10.1109/RadarConf2351548.2023.

[7] C. Schuessler, M. Hoffmann and M. Vossiek, "Super-Resolution Radar Imaging With Sparse Arrays Using a Deep Neural Network Trained With Enhanced Virtual Data," in IEEE Journal of Microwaves, vol. 3, no. 3, pp. 980-993, July 2023, doi: 10.1109/JMW.2023.3285610.

[8] S. S. Ahmed, "Microwave Imaging in Security — Two Decades of Innovation," in IEEE Journal of Microwaves, vol. 1, no. 1, pp. 191-201, Jan. 2021, doi: 10.1109/JMW.2020.3035790.

[9] N. Mahmood, N. Ghorbani, N. F. Troje, G. Pons-Moll, and M. J. Black, 'AMASS: Archive of Motion Capture as Surface Shapes', arXiv [cs.CV]. 2019.